The representation of symmetry in multi-voxel response patterns and functional connectivity throughout the ventral visual stream

Chayenne Van Meel [a], Annelies Baeck [a], Céline R. Gillebert [a,b,c], Johan Wagemans [a,b], Hans P. Op de Beeck [a,b,*]

[a] *Brain and Cognition, KU Leuven, Leuven, Belgium*
[b] *Leuven Brain Institute, KU Leuven, Leuven, Belgium*
[c] *Department of Experimental Psychology, University of Oxford, Oxford, United Kingdom*

A B S T R A C T

Several computational models explain how symmetry might be detected and represented in the human brain. However, while there is an abundance of psychophysical studies on symmetry detection and several neural studies showing where and when symmetry is detected in the brain, important questions remain about how this detection happens and how symmetric patterns are represented. We studied the representation of (vertical) symmetry in regions of the ventral visual stream, using multi-voxel pattern analyses (MVPA) and functional connectivity analyses. Our results suggest that neural representations gradually change throughout the ventral visual stream, from very similar part-based representations for symmetrical and asymmetrical stimuli in V1 and V2, over increasingly different representations for symmetrical and asymmetrical stimuli which are nevertheless still part-based in both V3 and V4, to a more holistic representation for symmetrical compared to asymmetrical stimuli in high-level LOC. This change in representations is accompanied by increased communication between left and right retinotopic areas, evidenced by higher interhemispheric functional connectivity during symmetry perception in areas V2 and V4.

1. Introduction

Humans and many other animals are highly sensitive to symmetry in visual patterns (Giannouli, 2013; Royer, 1981; Osorio and Cuthill, 2015; Treder, 2010; Wagemans, 1997). However, the detection and representation of symmetry is not an easy challenge for the underlying neural network (for an overview, see Bertamini and Makin, 2014; Bertamini et al., 2018). Initial visual processing is local, starting with the photoreceptor array in the retina and continuing up to primary visual cortex (V1) and even its surrounding areas V2 to V4. Certain computational models have suggested that symmetry might be detected by the analysis of correspondence of potentially symmetrical positions by areas such as V1 and V2 (e.g. Osorio, 1996; Zhu, 2014). However, with a complex visual pattern the analysis of all possible pairs of position would suffer from a combinatorial explosion, resulting in a variant of the famous correspondence problem for binocular vision (Marr, 1982; Julesz, 1971). For this reason it has been proposed that the correspondences would be established at the level of more complex shape features such as represented in areas higher up in the visual hierarchy, including V4 or even

beyond in object-selective cortex (Poirier and Wilson, 2010; Wagemans et al., 1993).

Despite these predictions about neural architecture, there is surprisingly little empirical evidence on the neural processing of symmetry and on how symmetrical patterns are represented. Indeed, as far as we know there is very little single-neuron work on this topic. Pramod and Arun measured single neuron responses in monkey IT cortex and found very similar responses to symmetrical and asymmetrical shapes, for instance, demonstrating part-based representations for both. The only notable difference was that symmetrical shapes were more distinctive from each other compared to asymmetrical shapes (Pramod and Arun, 2018). There is important work with fMRI in monkeys and humans (Sasaki et al., 2005; Tyler et al., 2005; Chen et al., 2007; Keefe et al., 2018), which has shown that symmetrical dot patterns are associated with higher responses in areas such as V4 and object-selective cortex. For example, in a recent study Keefe et al. (2018) showed symmetry selective BOLD responses in V3 and more ventral regions for frontoparallel and slanted symmetry. The same study found neural responses to depend on coherence and number of folds. Probably the best known aspect of symmetry is its

---

timing, thanks to a series of EEG experiments (Alp et al., 2018; Kohler et al., 2016; Makin et al., 2013, 2014, 2016). However, these results do not reveal how the visual patterns are represented or how the symmetry perception is related to detecting correspondences. Nor are the results directly relevant to confirm or reject the proposed computational models.

Here we report two fMRI experiments designed to investigate how symmetry perception is related to visual representations and neural communication between specific brain regions, which we regard as the two most wanted pieces of knowledge at the moment. We focus upon mirror symmetry around the central vertical meridian, which perceptually is the most salient type of symmetry (Treder, 2010; Wagemans, 1997). The first experiment is designed for representational analyses of multi-voxel patterns. These analyses can tell us in which regions we see a difference in how symmetrical and asymmetrical visual patterns are represented, and even what type of coding scheme is used for these patterns, such as part-based versus holistic coding (Kubilius et al., 2015). A second experiment is designed to investigate how functional connectivity is related to the perception of symmetry. Computational models have emphasized the role of analyzing corresponding positions in the visual display. In the case of centrally presented vertical mirror symmetry, the corresponding positions are located in separate hemifields. Therefore, we predict an increase in functional connectivity between left and right hemifield representations. Different models make different predictions about whether this would be found in the earliest cortical areas (Osorio, 1996) or V4 and later areas (Poirier and Wilson, 2010; Rhodes et al., 2005; Wagemans et al., 1993).

2. Materials and methods

2.1. Participants

Sixteen paid volunteers (age range 18–31 years; three male) with normal or corrected-to-normal vision participated in the experiment. The experiment was approved by the ethical committee of the Faculty of Psychology and Educational Sciences and the Medical Ethical Committee of the KU Leuven. Participants gave written consent at the start of each imaging session.

2.2. Stimuli

Stimuli consisted of white dot patterns presented on a dark grey background. Each dot pattern was generated using 150 dots, with each dot having a diameter of approximately 0.16 degrees of visual angle (d.v.a.) presented on a dark grey vertical rectangle (12 × 6 d.v.a.). The minimum distance between the individual dots was 1.4 times the dots' width. The minimum distance between the dots and the borders of the stimuli was half the minimum distance between the dots.

For the event-related MVPA runs, we first created four unique dot patterns. The four dot patterns were used to create three types of stimuli: parts, symmetrical stimuli and asymmetrical stimuli (Fig. 1). Part stimuli corresponded to the individual dot patterns and their mirror images. In the rest of the paper, these individual dot patterns will thus be referred to as "parts". Symmetrical and asymmetrical stimuli (size: 12 × 12 d.v.a.) were composed of two parts. Four symmetrical stimuli were created by combining each of the four parts with their mirror image. This resulted in one-fold symmetry along the vertical axis. The eight asymmetrical stimuli consisted of one of the four parts on the left side and the mirror image of a different part on the right side. This resulted in a total of 20 different stimuli per participant (see Table 1). The composition of the stimuli was balanced, with each part and its mirror image being included an equal number of times.

Note that for MVPA each stimulus corresponds to a condition in the fMRI design. To obtain a sufficient amount of repeats per condition/stimulus, we designed the experiment to have not more than 20 stimuli per participant. However, we created an independent set of dot patterns per pair of participants. Thus, across all participants, the results are based
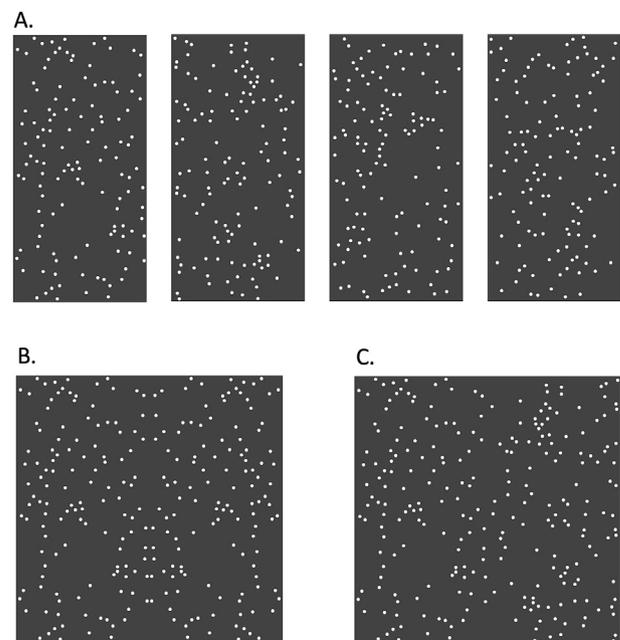

Fig. 1. Examples of dot pattern stimuli used in the experiment. A) Four individual dot patterns (or "parts"). For each pair of participants, a different set of dot patterns was created. Individual dot patterns and their mirror images were presented as part stimuli during the MVPA runs. B) A symmetrical stimulus consisting of the first dot pattern shown in panel A and its mirror image. C) An asymmetrical stimulus consisting of the first dot pattern and the mirror image of the second dot pattern shown in panel A.

Table 1
Composition of the 20 stimuli used in the MVPA runs. For cells appearing in grey in this table, an example stimulus is shown in Fig. 1.

stimulus number	left side	right side
left parts		
1	part 1	
2	part 2	
3	part 3	
4	part 4	
right parts		
5		mirrored part 1
6		mirrored part 2
7		mirrored part 3
8		mirrored part 4
symmetrical		
9	part 1	mirrored part 1
10	part 2	mirrored part 2
11	part 3	mirrored part 3
12	part 4	mirrored part 4
asymmetrical		
13	part 1	mirrored part 2
14	part 1	mirrored part 3
15	part 2	mirrored part 3
16	part 2	mirrored part 4
17	part 3	mirrored part 4
18	part 3	mirrored part 1
19	part 4	mirrored part 1
20	part 4	mirrored part 2

upon a large set of images, which avoids that the findings depend on the specifics of a small subset of dot configurations.

For the functional connectivity runs (described below), a new set of 60 parts was created using the same parameters. The parts were used to create 60 unique symmetrical and 60 unique asymmetrical stimuli, again

controlling for the number of presentations of the individual parts and their mirror images.

2.3. Imaging parameters

Imaging data were acquired using a 3T Philips Ingenia CX scanner with a 32-channel head coil at the Department of Radiology of KU Leuven. Each functional run consisted of T2*-weighted echoplanar images (EPIs) (32 slices, resolution $2 \times 2 \times 2$ mm, interslice gap 0.1 mm, TR = 2 s, TE = 30 ms, 104×104 acquisition matrix). For the localizer runs TR = 3 s, while all other imaging parameters remained the same. In addition to the functional images a high-resolution T1-weighted anatomical scan was collected for each participant (182 slices, resolution $0.98 \times 0.98 \times 1.2$ mm, TR = 9.6 ms, TE 4.6 ms, 256×256 acquisition matrix).

2.4. Experimental procedure

The experiment consisted of two 2-hour scanning sessions per participant. Over the course of these sessions, all participants completed 1 training run, between 10 and 15 MVPA runs, 4 connectivity runs, 2 localizer runs and 2 meridian mapping runs. Except for the training run, the runs were semi-randomly interleaved, with the restriction that about half of the MVPA runs and connectivity runs were presented in each session. Localizer runs and meridian mapping runs were not split up over the two sessions. Note that the runs have been named after the associated analysis method. Participants received instructions about all tasks before entering the scanner room. At the start of each run, the instructions for the task at hand were repeated. Stimuli were presented using Psychtoolbox 3 (Brainard, 1997) via an NEC projector with a NP21LP lamp that projected the image on a screen the participant viewed through a mirror mounted on the head coil. Viewing distance was approximately 64 cm. In all types of runs, the presentation order of the conditions was counterbalanced over runs and over participants. During the MVPA runs and connectivity runs, eye movements were recorded by tracking one of the pupils with the MR compatible EyeLink 1000 Plus eye tracking system. At the beginning of each session, we emphasized that it was important to maintain central fixation during all runs.

2.4.1. Training run

The first imaging session started with one MVPA test run to acquaint the participants with the stimuli and task. Data of this training run were not included in the analysis. When the training run was completed, participants received feedback on their behavioral performance, and most importantly, about their fixation performance. Feedback was not provided to participants in any of the subsequent runs.

2.4.2. MVPA runs

In the MVPA runs, a rapid event-related design was used to schedule the presentation of the stimuli. On each trial, a dot pattern was presented for 1 s with a jittered inter-stimulus interval (ISI) of between 3 and 11 s. The ISI and order of the stimuli were scheduled using optseq2 (Dale, 1999) and were varied across participants. A red fixation dot was presented in the center of the screen for the full duration of each run. Total duration of each event-related MVPA run was 400 s. Participants were presented with 20 different stimuli (see 2.2): 4 parts presented on the left side of the fixation dot, 4 mirrored parts presented on the right side, 4 symmetrical stimuli and 8 asymmetrical stimuli. Within one run, each of the 20 stimuli was presented four times. The luminance of the dot patterns varied over trials, such that half of the trials contained "light" dot patterns, while the other half contained "dark" dot patterns. On "light" trials, the dots were white. On "dark" trials, the difference in greyscale between dots and background was reduced to a fourth of the difference in the "light" trials, resulting in grey dots. The background luminance remained unchanged across trials. Participants had to indicate whether the luminance of the dot pattern in the current trial was the same or

different compared to the luminance of the dot pattern in the previous trial. No answer was required on the first trial in a run.

2.4.3. Connectivity runs

In the connectivity runs a block design was used consisting of four blocks of symmetrical stimuli and four blocks of asymmetrical stimuli. Participants were presented with 60 different symmetrical and 60 different asymmetrical stimuli, with 15 stimuli per block. Each stimulus was presented for 1 s with 1 s ISI. These stimulus blocks were alternated with three fixation blocks: in the beginning, middle and at the end of each run. Each block lasted 30 s, making the total duration of each run 330 s. A red fixation dot was presented centrally throughout each run, while participants performed a passive fixation task.

2.4.4. Localizer runs

Each localizer run consisted of four blocks of grayscale pictures of objects, four blocks of phase-scrambled images, and five fixation blocks. Each block lasted 15 s. A stimulus block contained 20 images, consisting of 18 different images and 2 immediate repeats, which were presented for 300 ms each with a 450 ms ISI. Participants performed a one-back repetition detection task. Six of the participants previously participated in an earlier unpublished study and localizer data obtained in that study was reused in the current experiment.

2.4.5. Meridian mapping runs

In the meridian mapping runs, a standard procedure from Tootell et al. (1995) was adopted. We presented eight 15 s blocks of horizontal and eight 15 s blocks of vertical checkerboard wedges, varying in the shapes within the wedges, as well as the number, size and color of the different shapes within the wedges. The checkerboard wedges were presented for 250 ms, with a 125 ms ISI. The checkerboard blocks were alternated with 9 fixation blocks of 15 s. Participants were asked to detect changes in the size of the fixation dot.

3. Data analyses

3.1. Quality of fixation

The quality of the recorded eye movement data was insufficient for quantitative data analyses (low signal to noise and high levels of drift), due to a technical issue in our setup at the time (shadow cast by the RF coil). The pupil was nevertheless clearly visible to the experimenter during scanning. Based on observations during the scan sessions, the experimenter noted on the protocol sheet that two participants were not sufficiently fixating on the central fixation point. If so, then one would predict no clear differences between stimuli in how they activate the retinotopic maps in visual cortex. To verify this we performed preliminary analyses in all participants using an approximate definition of V1 (using a probability map from the SPM anatomy toolbox). Decoding performances for two whole stimuli in V1 in these two participants were very poor and outliers compared to the decoding performances in the V1 ROI in other participants (51.62% and 56.85% versus on average 83.15% with SD 7.73% in the other participants). Therefore, data from these two participants were discarded before further analysis.

3.2. Preprocessing and general linear model

Imaging data of all functional runs were preprocessed and analyzed using the Statistical Parametric Mapping software package (SPM8, Wellcome Department of Cognitive Neurology, London). Preprocessing steps involved slice timing correction, spatial realignment, co-registration of functional and anatomical images and spatial normalization to an MNI (Montreal Neurological Institute) template using a 4th degree B-spline interpolation. During normalization, functional images were re-sampled to a voxel size of $2 \times 2 \times 2$ mm. Functional images were then smoothed using Gaussian kernels of 4 mm full-width at half maximum (FWHM).

A General Linear Model (GLM) was applied to the preprocessed images at an individual level in each voxel and run. The GLM of the MVPA runs included 20 regressors for the experimental conditions (i.e. 20 independent variables corresponding to the different stimuli), and six regressors for the motion correction parameters (regressors for the motion correction parameters (x,y,z for translation and rotation, extracted during preprocessing) as covariates of no experimental interest. Further analyses (see 3.5 Multi-voxel pattern analysis) were performed using the t-statistics (resulting from the contrast of each condition versus baseline; Misaki et al., 2010) per run obtained after fitting the general linear model. The GLM of the connectivity runs consisted of 2 regressors for the conditions (i.e. symmetrical and asymmetrical) and six regressors for the motion correction parameters. For the localizer runs, the GLM included 2 regressors for objects and scrambled images and six motion correction regressors. The GLM of the meridian mapping runs included a regressor for horizontal wedges, one for vertical wedges, and six motion correction regressors.

3.3. Regions of interest

Multiple visual regions along the ventral visual stream were selected as regions of interest (ROI): V1, V2, V3, V4, and the lateral occipital complex (LOC; Fig. 2).

Regions V1, V2, V3, and V4 were defined in surface space. FreeSurfer (http://surfer.nmr.mgh.harvard.edu/, Martinos Center for Biomedical Imaging, Harvard-MIT, Boston USA) was used to reconstruct and inflate subjects' cortical surfaces from the anatomical images (Dale et al., 1999; Fischl and Dale, 2000). Each subject's anatomy was registered to the fsaverage-sym template space (Fischl et al., 1999; Greve et al., 2013). A template of Benson et al. (2014) was used to delineate V1, V2, and V3. This template accurately predicts the location and retinotopic organization of these early visual areas from individuals' cortical anatomy alone. Although this template's prediction errors are very low overall, the prediction of polar angle is somewhat less accurate near the foveal confluence as well as near the outer borders of V3. With this in mind, we included only the part of the template extending from 1.5° to 10° eccentricity. Moreover, we used the functional data of the meridian mapping runs to define the horizontal and vertical meridians for each subject, by means of the horizontal minus vertical wedges contrast. In cases where the outer borders of V3 according to the template deviated from the second vertical meridian (i.e. the functionally defined outer border of V3), the border was adjusted to fit the functional data. Area V4 was defined as sharing a border with ventral V3, and extending ventrally up until the posterior transverse collateral sulcus (ptCoS; Witthoft et al., 2014). In theory, V4 extends laterally until the lower vertical meridian. This meridian, however, may be hard to image due to an MR artefact

caused by the nearby transverse sinus (Winawer et al., 2010). In multiple subjects, we did indeed not see a clearly defined lower vertical meridian. In these cases, we defined the lateral boundary of V4 as lying beyond the functionally defined horizontal meridian. Regions V1, V2, V3 and V4 were then converted from surfaces to volume space.

The high-level visual region LOC was defined in volume space by a combination of functional data from the localizer scans and anatomical landmarks. The lateral occipital complex (LOC) was defined by the objects minus phase-scrambled images contrast. Only lateral occipital and occipitotemporal regions were included. The threshold for all contrasts was p < 0.0005 (uncorrected for multiple comparisons).

3.4. Univariate analysis

We verified if we could replicate univariate findings from previous research on symmetry in an event-related design as well as in a block design. We compared the univariate responses (beta values) to symmetrical stimuli, asymmetrical stimuli and parts in the MVPA runs for each ROI separately using paired t-tests. We also compared the univariate response (beta values) to blocks of symmetrical stimuli and blocks of asymmetrical stimuli during the connectivity runs using a paired t-test. The α-level was Bonferroni corrected within ROIs, resulting in α = 0.0166 for results of the MVPA runs and α = 0.05 for results of the connectivity runs.

3.5. Multi-voxel pattern analysis

Support vector machines (SVM) were implemented using custom Matlab code and the OSU SVM Matlab toolbox. Multi-voxel response patterns were extracted per ROI for every stimulus in each of the MVPA runs for each participant. The responses were standardized using a standard-normal transformation across voxels. For each pair of stimuli, a linear SVM was trained to determine the hyperplane that best separates the data from these two stimuli using the response patterns from a subset (approximately 70%) of the runs. The following parameters were used: a radial basis function kernel as decision function (gamma set to 1) and a C-SVS classification algorithm (C set to 1). The performance of the classifier on this pair-wise classification was then calculated for the average data from the remaining runs. This procedure was repeated 100 times per pair of stimuli with a random assignment of runs to the training and test set, and performance was averaged over all repetitions. This resulted in a 20×20 decoding matrix for each ROI and each participant. The higher the decoding accuracy, the better the classifier is able to discriminate between the two stimuli, indicating more distinct neural representations.

Specific hypotheses were tested by averaging over the relevant cells of the individual decoding matrices, and subsequently using pairwise t-tests. Note that only the values in the upper triangular are used. We compared decoding performance within stimulus categories (symmetrical versus symmetrical, asymmetrical versus asymmetrical) and across categories (symmetrical versus asymmetrical). By definition, two different symmetrical stimuli differ from each other in both parts. To make sure that effects would be purely related to the stimulus category, we likewise only included the decoding performance for stimulus distinctions in which stimuli differed in both parts to calculate the two other decoding levels (asymmetrical versus asymmetrical and symmetrical versus asymmetrical). In addition we directly compared decoding performance for stimuli differing in both parts to decoding performance for stimuli sharing one identical part in the same location (left/right), both within category (asymmetrical versus asymmetrical) and across category (symmetrical versus asymmetrical). This analysis provides insight into the extent to which the underlying stimulus representations are part-based. These analyses were performed separately for each ROI. The α-level was Bonferroni corrected within ROIs per research question, resulting in α = 0.0166 and α = 0.025 for effects of stimulus category and shared parts respectively.
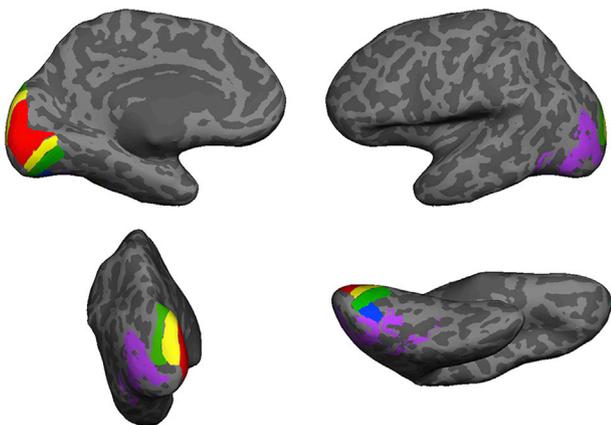

Fig. 2. Regions of interest (ROI). One subject's ROIs are shown on that subject's inflated left hemisphere. V1 is shown in red, V2 in yellow, V3 in green, V4 in blue and LOC in purple. Visualized using Freesurfer (Fischl et al., 1999).

3.6. Functional connectivity analysis

The functional connectivity analysis was carried out using custom Matlab scripts (see Bulthé et al., 2018). As we were interested in inter-hemispheric connectivity, each of our five ROIs was separated into a left-hemisphere and right-hemisphere part. The input for this analysis was the unsmoothed normalized data of the connectivity runs. Pre-processing steps for the functional connectivity analysis were (in this order) scrubbing, high-pass filtering above 0.01 Hz, regressing out the white matter and ventricle signals, regressing out head motion, removing the contribution of task-evoked activity using the regressors for the symmetrical and asymmetrical condition, low-pass filtering below 0.2 Hz, and spatial smoothing at 4 mm FWHM. As we subtracted the task-evoked BOLD response, the residual signal reflects the intrinsic brain activity. For each subject, time courses for this residual intrinsic response were extracted per condition (symmetrical and asymmetrical) and averaged over voxels within a ROI. Functional connectivity was computed within subjects by calculating Pearson cross-correlation between the BOLD time courses of each pair of ROIs, and converting the correlations to Z-scores (Fisher's r-to-Z transformation). This resulted in two 10×10 connectivity matrices per subject. For each condition, these matrices were averaged over subjects to create one group-level 10×10 connectivity matrix.

The functional connectivity analyses were designed to measure the consequences of correspondence analysis in symmetry detection, in which potentially symmetrical points are compared. Given that this study focuses on mirror symmetry around a vertical axis and that the stimuli are presented centrally, the potentially symmetrical points are always located in separate hemifields. Hence, the perception of symmetry could influence the coordination between hemispheres. Therefore, we focused on functional connectivity values of the homotopic interhemispheric connections (lV1-rV1, lV2-rV2, lV3-rV3, lV4-rV4, lLOC-rLOC) and averaged over these five connections to get an overall measure of inter-hemispheric connectivity. We then compared overall interhemispheric connectivity during symmetrical blocks and asymmetrical blocks using a paired t-test. Additionally, we compared connectivity during symmetrical and asymmetrical blocks for each of the five connections separately, using paired t-tests (FDR-corrected, $\alpha = 0.05$).

4. Results

4.1. Differences in mean activation

During the MVPA runs, univariate responses were enhanced for symmetrical compared to asymmetrical stimuli in V4 ($t(13) = 3.8007$, $p = 0.0022$) and LOC ($t(13) = 5.1330$, $p = 0.0002$), but not in earlier regions (V1: $t(13) = -0.2715$, $p = 0.7903$; V2: $t(13) = -0.6046$, $p = 0.5559$; V3: $t(13) = 1.1765$, $p = 0.2605$, paired t-tests). In LOC, the response to asymmetrical stimuli even decreased to the level of activation for parts ($t(13) = 0.7408$, $p = 0.472$). In all other regions, responses were higher for all whole stimuli (symmetrical and asymmetrical) compared to parts (all $p < 0.0001$, paired t-tests, Fig. 3A).

During the connectivity runs, univariate responses were enhanced for blocks of symmetrical stimuli compared to blocks of asymmetrical stimuli in V3 ($t(13) = 4.7658$, $p = 0.0004$), V4 ($t(13) = 9.9709$, $p < 0.0001$), and LOC ($t(13) = 8.9429$, $p < 0.0001$), but not in V1 ($t(13) = 1.5996$, $p = 0.1337$) and V2 ($t(13) = 1.6934$, $p = 0.1142$, paired t-tests, Fig. 3B).

These findings confirm results from earlier studies about differences in univariate levels of activation between symmetrical and asymmetrical dot patterns (Sasaki et al., 2005; Tyler et al., 2005; Chen et al., 2007; Keefe et al., 2018).

4.2. Multi-voxel representations of symmetrical and asymmetrical patterns

In early visual regions V1 and V2, decoding performance did not depend on whether a dot pattern was symmetrical or asymmetrical.
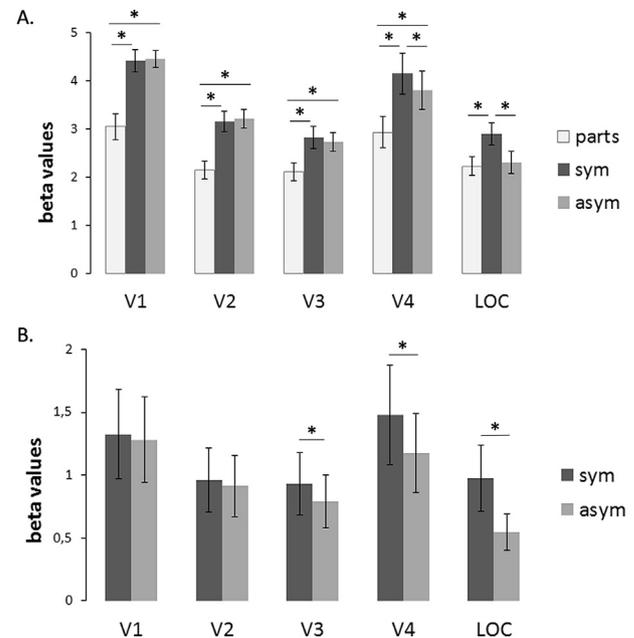

Fig. 3. Mean activation across subjects in each of the ROIs. A) Beta estimates for parts, symmetrical and asymmetrical stimuli in the MVPA runs. B) Beta estimates for symmetrical and asymmetrical stimuli in the functional connectivity runs. Error bars denote the standard error of the mean (SEM) across subjects. sym: symmetrical, asym: asymmetrical. * panel A: $p < 0.0166$, panel B: $p < 0.05$.

Accuracy was equally high for symmetrical versus symmetrical stimuli (V1: 88.04%; V2: 80.08%), and asymmetrical versus asymmetrical stimuli (V1: 86.54%, $t(13) = 1.055$, $p = 0.3106$; V2: 77.53%, $t(13) = 1.6167$, $p = 0.1299$, paired t-tests). Decoding accuracy also did not differ for symmetrical versus asymmetrical stimuli (V1: 88.17%; V2: 80.08%) compared to either symmetrical versus symmetrical stimuli (V1: $t(13) = -0.1261$, $p = 0.9016$; V2: $t(13) = 0.0066$, $p = 0.9948$) or asymmetrical versus asymmetrical stimuli (V1: $t(13) = 2.0107$, $p = 0.0656$; V2: $t(13) = 1.8988$, $p = 0.08$, paired t-tests, Fig. 4A). However, decoding performance depended heavily on whether or not the stimuli had one part in common. For across-category comparisons (i.e. symmetrical versus asymmetrical), accuracy dropped approximately 10% (V1: 10.32%, $t(13) = -15.16$, $p < 0.0001$; V2: 11.41%, $t(13) = -12.763$, $p < 0.0001$, paired t-tests) when stimuli shared an identical part in the same location. For within-category distinctions (i.e. asymmetrical versus asymmetrical), accuracy also decreased approximately 10% (V1: 11.42%, $t(13) = -8.7622$, $p < 0.0001$; V2: 10.15%, $t(13) = -5.7855$, $p < 0.0001$, paired t-tests, Fig. 4B). These findings suggest a part-based code that does not capture that symmetrical dot patterns are somehow different compared to asymmetrical dot patterns.

High up the ventral stream, the pattern of results looks very different. In LOC, decoding accuracy was higher across categories (70.39%) than for stimuli of the same category, whether those were symmetrical (61.51%, $t(13) = -4.5824$, $p = 0.0005$) or asymmetrical (56.43%, $t(13) = 5.6196$, $p < 0.0001$, paired t-tests). Within categories, however, discriminability for two symmetrical stimuli did not differ significantly from discriminability for two asymmetrical stimuli ($t(13) = 2.206$, $p = 0.046$, paired t-test, Fig. 4A). Moreover, classification performance for two asymmetrical stimuli decreased to 52.61% when the stimuli shared a part ($t(13) = -2.6651$, $p = 0.0194$), but there was no drop in performance for symmetrical versus asymmetrical stimuli that shared a part ($t(13) = 0.2791$, $p = 0.7846$, paired t-tests, Fig. 4B). These findings suggest a more holistic representation for symmetrical stimuli that also captures that symmetrical dot patterns are very different compared to asymmetrical dot patterns.

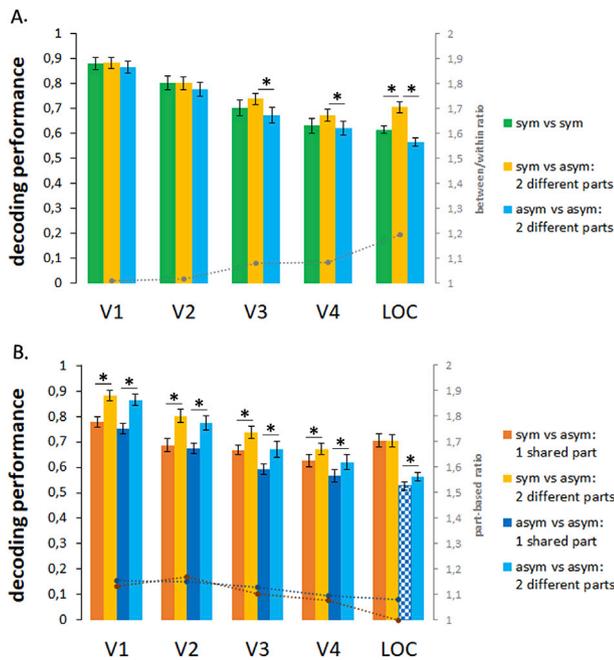Interestingly, an intermediate pattern was found in V3 and V4. Like

Fig. 4. Mean decoding performance (expressed as proportion correct) across subjects in each of the ROIs. A) Mean decoding performance for between-category (sym vs asym, yellow) and within-category (green, blue) stimulus pairs that differ in both parts. The grey dotted line reflects the "between/within" ratio (see text). B) Mean decoding performance for between-category (orange-yellow) and within category (dark blue-blue) stimulus pairs as a function of whether or not the stimuli share a part. Checkboard patterns indicate that performance is not significantly above chance level. The dark orange and dark blue dotted line reflect the "part-based ratio" for between and within category stimuli, respectively. Error bars denote the standard error of the mean (SEM) across subjects. sym: symmetrical, asym: asymmetrical. * panel A: p < 0.0166, panel B: p < 0.025.

LOC, these regions show better decoding for stimuli across category (V3: 73.76%; V4: 67.19%) than for two asymmetrical stimuli (V3: 67.14%, $t(13) = 4.7457$, $p = 0.0004$; V4: 62.04%, $t(13) = 2.8836$, $p = 0.0128$, paired t-tests, Fig. 4A). On the other hand, like in early regions, classification was always better when stimuli did not share a part. For symmetrical versus asymmetrical classification, accuracy dropped 6.93% ($t(13) = -6.9027$, $p < 0.0001$) and 4.54% ($t(13) = -5.0483$, $p = 0.0002$, paired t-tests) for V3 and V4, respectively. For two asymmetrical stimuli, performance decreased 7.89% ($t(13) = -5.6082$, $p < 0.0001$) and 5.36% ($t(13) = -3.6851$, $p = 0.0027$, paired t-tests) for V3 and V4 respectively (Fig. 4B).

For visualization purposes, two ratios were also computed and plotted on the relevant bar graphs. Ratios were calculated per subject and subsequently averaged. The ratio plotted in Fig. 4A (grey dotted line) is the "between/within ratio", calculated as the decoding performance of symmetrical vs. asymmetrical stimuli (i.e. between category decoding) divided by the average of the decoding performances for symmetrical vs. symmetrical and asymmetrical vs. asymmetrical stimuli (i.e. within-category decoding). Higher ratios indicate a higher availability of category information. A between/within ratio of 1 implies that the representations contain no information about the category beyond what is already represented in the differences between stimuli within these categories. Note that we see an increase in this ratio throughout the ventral visual stream. The ratios plotted in Fig. 4B (dark orange and blue dotted lines) reflect the "part-based ratio" for between and within category stimuli, respectively. This ratio is calculated by dividing decoding performance for stimuli that do not share a part by that of stimuli that share 1 part in the same location. A part-based ratio of 1 indicates the absence of a drop in performance due to sharing a part. Higher values

indicate higher drops in performance and thus a more part-based representation. It can be seen in Fig. 4B that the part-based ratio decreases throughout the ventral visual stream. Additionally, supplementary Figs. S1–2 contain MDS plots representing the neural similarity between the stimuli.

4.3. Functional connectivity

Given that the detection of symmetry in computational models is based upon establishing the correspondence between individual points, which in this case comes down to sub-patterns in the left and right hemifield, we expect to see higher levels of functional connectivity between corresponding regions in left and right hemisphere.

Overall, taking all five left-right pairs of ROIs together, Interhemispheric connectivity was higher during presentation of blocks of symmetrical stimuli compared to asymmetrical stimuli ($t(13) = 2.3055$, $p = 0.0191$, paired t-test).

When comparing connectivity between symmetrical and asymmetrical blocks for each homotopic connection separately, we found a difference for V2 ($t(13) = 4.8188$, $p = 0.0002$, paired t-test) and V4 ($t(13) = 2.7994$, $p = 0.0075$, paired t-test), but not for the other connections (all FDR-corrected $p > 0.05$, Fig. 5).

These results indicate that the correspondence analysis of potentially symmetrical points in visual space likely occurs in multiple locations within the ventral visual pathway, namely in V2 and V4. This pattern of results shows both similarities and differences with the results of our univariate and multivariate analyses reported above. On the one hand, while area V2 showed a strong change in functional connectivity, symmetry did not affect the activation level or neural representations in this region. The reverse is true for V3 and LOC: These regions showed increased activation and distinguishable multi-voxel patterns for symmetrical compared to asymmetrical stimuli, but no functional connectivity effect. On the other hand, functional connectivity and MVPA results both seem to suggest that symmetry processing does not happen at just one level in the cortical hierarchy but gradually (MVPA) and at multiple levels.
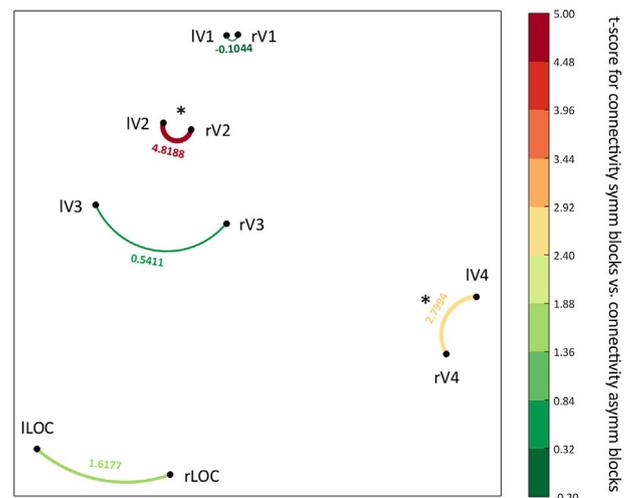

Fig. 5. Multidimensional scaling (MDS) plots of the ROIs' functional connectivity. Connectivity matrices during symmetrical and asymmetrical blocks were averaged and then used as similarity measure for MDS. MDS was performed using Matlab's mdscale function, with 2 dimensions and the default stress criterion. The closer ROIs are to each other in the figure, the higher their connectivity. Colored lines reflect changes in functional connectivity, expressed as the t-value resulting from the paired t-test for symmetrical compared to asymmetrical blocks for each of the homotopic interhemispheric connections. Warmer colors and thicker lines reflect higher values. *p < 0.05 FDR corrected.

4.4. Lateralization of symmetry selectivity

The results reported in Sections 4.1 and 4.2 are based on activation levels and multi-voxel patterns in bilateral ROIs. In other words, we did not split up ROIs into left and right hemisphere prior to the univariate and multivariate analyses. However, given a long-term debate in the symmetry literature on whether or not there is a right hemisphere advantage for symmetry perception, we looked into hemispheric differences in symmetry selectivity a posteriori.

For the univariate data, we compared the difference in mean activation for symmetrical and asymmetrical patterns between the two hemispheres for regions of interest in which we found a selective response (i.e. significantly higher activation for symmetrical compared to asymmetrical stimuli). In the event-related data we found lateralization of symmetry selectivity in V4 ($t(13) = -3.6430$, $p = 0.003$) and LOC ($t(13) = 3.8116$, $p = 0.0021$, paired t-tests). However, in V4 this effect was in the unexpected direction (more symmetry detection in the left hemisphere). In the block design data we found lateralization in V3 ($t(13) = 4.0599$, $p = 0.0014$) and LOC ($t(13) = 5.8521$, $p < 0.0001$), but not in V4 ($t(13) = -0.5305$, $p = 0.6047$, paired t-tests).

For the MVPA data, we compared decoding performance for symmetrical versus asymmetrical performance between hemispheres for regions of interest in which between-category decoding outperformed within-category decoding, as we felt this comparison conceptually gets closest to the comparison in the univariate data. In V3 and V4, no difference in symmetrical versus asymmetrical decoding performance was observed between the hemispheres, whether the stimuli shared a part or not (V3: shared part $t(13) = 1.7007$, $p = 0.1128$, 2 different parts $t(13) = 0.0192$, $p = 0.985$; V4: shared part $t(13) = -1.1803$, $p = 0.259$, 2 different parts $t(13) = -0.7019$, $p = 0.4951$, paired t-tests). We did find a right lateralization in LOC when stimuli shared a part ($t(13) = 3.6083$, $p = 0.0032$) and when both parts were different ($t(13) = 2.8593$, $p = 0.0134$, paired t-tests).

Our data thus show a consistent right lateralization of symmetry selectivity in LOC, in terms of overall response strength (replicated in two designs) as well as in multi-voxel selectivity. Results for earlier regions are inconclusive.

5. Discussion

We presented participants with symmetrical and asymmetrical dot patterns and the parts, or halves, which they were made up of. In agreement with results of earlier fMRI studies (Sasaki et al., 2005; Tyler et al., 2005; Chen et al., 2007; Keefe et al., 2018), we found increased levels of activation in high-level visual areas for symmetrical compared to asymmetrical stimuli, but no differences in activation levels were observed in early visual cortex. Notably, the brain region where the activation difference first appeared varied depending on the design that was used. In our event-related data, the difference was seen in V4 and LOC, whereas it was already evident as early as V3 in the block design data. This result is in accordance with the notion that theoretically, block designs have greater statistical power than event-related designs (Friston et al., 1999), and are thus well suited to detect differences in activation between experimental conditions.

We note that our univariate results differ from those reported in a recent study by Pramod and Arun (2018). This study is relevant as it also looked at the relationship between parts and wholes in objects, with asymmetrical objects consisting of the same parts used to form the symmetrical objects. Pramod and Arun (2018) did not find any difference in activation between symmetrical and asymmetrical stimuli. We presume that this difference in outcome might be caused by the use of a different type of stimuli. They presented participants with object stimuli instead of dot patterns. We assume that the detection of symmetry in dot patterns might result in these dot patterns being perceived as a figure, or object, and that this is not the case for asymmetrical dot patterns. This difference in figure-ground segregation is not applicable to the stimuli of

Pramod and Arun (2018) as those are all objects to begin with.

While it is important to note that the univariate findings of earlier studies using dot pattern stimuli were replicated here, the primary goal of this study was to investigate how symmetrical and asymmetrical visual patterns are represented, and which brain regions are involved in detecting the correspondence between symmetrical points in the visual field. The combined use of MVPA and functional connectivity analyses in this study allows us to provide a first answer to these questions that have been left unexplored by previous fMRI and EEG experiments. By using multi-voxel patterns as input, MVPA retains information that is averaged out in univariate analyses. Moreover, MVPA was well suited to investigate in a systematic way how representations of whole stimuli are related to the representations of their constituent parts and how this relation changes throughout the ventral stream. Furthermore, functional connectivity analyses provide valuable insight into whether and how detecting a match between corresponding positions in separate halves of visual space might increase cooperation between the brain regions in which those halves are represented. In this study, stimuli were presented centrally and had one vertical symmetry axis, and thus corresponding positions are located in separate hemifields and primarily represented in separate hemispheres. Therefore, we focused on changes in interhemispheric connectivity.

The results from the multi-voxel pattern analyses suggest a gradual change from part-based to more holistic representations for symmetrical dot patterns throughout the ventral visual stream. In early regions V1 and V2, decoding performance was high overall and was independent of the category of the discriminated stimuli. This suggests that symmetrical and asymmetrical dot patterns share a representational code in these areas. Evidence that this shared code is part-based comes from the observation that decoding performance is much worse when the stimuli contain the same part in the same hemifield. We observed a general drop in performance over the course of the ventral visual stream. However, this drop was less pronounced for across-category stimulus pairs, which is reflected in better decoding performance for across-category stimulus pairs compared to one or both types of within-category stimulus pairs from V3 onwards. In other words, in extrastriate visual cortex representations of symmetrical and asymmetrical patterns become more and more dissimilar. Moreover, while in V3 and V4 representations for symmetrical as well as asymmetrical stimuli still prove to be part-based, a shared part does not hamper across-category decoding performance anymore in LOC. This suggests that stimuli are represented in a more holistic way higher up in the ventral stream. Given that two asymmetrical stimuli are slightly less well discriminated when they share a part even in LOC, this transformation from a part-based to a holistic code seems to be complete only for symmetrical stimuli.

These results are reminiscent of the findings in a study by Kubilius et al. (2011), which investigated the neural underpinnings of the configural-superiority effect. This study found that patterns in V1, V2 and V3 were more informative about parts than about wholes, but that classification was more accurate for wholes than parts in LOC. Moreover, in LOC part information was not represented in the wholes. This indicates that other holistic properties besides symmetry might also emerge gradually, with a crucial role for higher regions. The increase in holistic processing along the visual hierarchy is accompanied by an increase in receptive field size, and the question can be raised to what extent receptive field size is a sufficient explanation for our results. However, receptive field size alone cannot explain the differences in representation and in connectivity between symmetrical and asymmetrical patterns, which is the most important aspect of our results.

A different study from our lab (Baeck et al., 2013) looked into part-whole relationships in LOC for random and meaningful object pairs using, among other analyses, similar multi-voxel pattern analyses as reported here. Decoding accuracy dropped for pairs that had an object in common compared to accuracy for pairs with no common objects. It is thus not the case that LOC is incapable of representing information about parts within a whole, which is also illustrated by the representations of asymmetrical patterns in LOC in our study.

To investigate which brain areas are involved in detecting the correspondence between hemifields in the perception of centrally presented mirror symmetry, we performed functional connectivity analyses. Connectivity between hemispheres increased during the presentation of symmetrical stimuli compared to asymmetrical stimuli, specifically for V2 and V4. This indicates that the correspondence analysis likely involves computational steps in multiple brain regions and highlights the need for a model that combines an early filter process based on low-level features (e.g. Osorio, 1996; Zhu, 2014) detected by the complex cells in V2 and a later computation based on more complex features in V4, such as the convex/concave contour detection proposed by Poirier and Wilson (2010).

It should be noted that the representation of the ipsilateral field increases along the visual hierarchy. These factors might affect baseline correlations between hemispheres, and thus interhemispheric functional connectivity, and may interact differently with different stimulus conditions. Our results, however, show a nonlinear pattern with differences in connectivity between the symmetrical and asymmetrical condition only in V2 and V4, which seems inconsistent with an explanation in terms of the steady increase in ipsilateral representation.

As highlighted before, our focus on interhemispheric connectivity is justified given the stimuli used in this study. It is possible that cooperation between hemispheres is relevant either exclusively or especially for the type of symmetry used here, i.e. centrally presented mirror symmetry, and cannot explain correspondence analysis in symmetry detection in general. Rather, we consider it a special case of a more general process in which connectivity is increased between neural areas representing corresponding points in the stimulus (e.g. upper and lower visual hemifield representations for centrally presented horizontal reflection). Future studies which carefully map retinotopy for all regions of interest could test this claim for different types of symmetry. In the same vein, the univariate and multivariate results reported here could well reflect neural processes common to various types of symmetry, in which case future studies using different stimuli should find similar results. A first suggestion that neural measures of symmetry selectivity can indeed be generalized to different dot stimuli comes from two EEG studies. Wright, Makin, and Bertamini (2015) showed that the sustained posterior negativity (SPN) was comparable for vertical and horizontal reflection. In a later study (Wright et al., 2017) they showed that an SPN is also generated for symmetry presented only within the left or right hemifield.

There appears to be a general resemblance between the univariate results and MVPA results in this study. In particular, the brain regions that show higher activation for symmetrical stimuli are the same as the areas in which the representations for symmetrical and asymmetrical stimuli diverge. The functional connectivity results, however, differ from these observations in an important way. Among the regions that show a difference between symmetrical and asymmetrical patterns in activation level and neural representation, only V4 (and thus not V3 and LOC) also shows a functional connectivity effect. The most striking discrepancy, however, is observed in V2. While this region does not seem to contain any symmetry information based on the univariate and multivariate results, it shows the strongest connectivity effect. Despite these discrepancies, functional connectivity results and MVPA results both suggest that symmetry is a gradual process involving multiple computational steps at multiple levels. Although most models on symmetry detection are multi-stage models and some even directly refer to the processing hierarchy in the visual system (e.g. Poirier and Wilson, 2010), they tend to put forward a single feature as being critical for symmetry detection and do not explicitly relate the different processing stages they propose to different neural locations. New models of symmetry are needed which are biologically plausible and integrate elements of models that have already been proposed. This implies that such models should highlight the involvement of multiple brain regions and features – low-level as well as high-level – and their specific role in the computational hierarchy of symmetry detection to provide a comprehensive explanation for behavioral and neuroimaging findings alike.

Declarations of interest

The authors have no conflicts of interest.

Acknowledgements

Appendix A. Supplementary data

Supplementary data to this article can be found online at https://doi.org/10.1016/j.neuroimage.2019.02.030.

References

Alp, N., Kohler, P.J., Kogo, N., Wagemans, J., Norcia, A.M., 2018. Measuring integration processes in visual symmetry with frequency-tagged EEG. Sci. Rep. 8, 6969. http://doi.org/10.1038/s41598-018-24513-w.

Baeck, A., Wagemans, J., Op de Beeck, H.P., 2013. The distributed representation of random and meaningful object pairs in human occipitotemporal cortex: The weighted average as a general rule. Neuroimage 70, 37–47. https://doi.org/10.1016/j.neuroimage.2012.12.023.

Benson, N.C., Butt, O.H., Brainard, D.H., Aguirre, G.K., 2014. Correction of distortion in flattened representations of the cortical surface allows prediction of V1-V3 functional organization from anatomy. PLoS Comput. Biol. 10 (3), e1003538. http://doi.org/10.1371/journal.pcbi.1003538.

Bertamini, M., Makin, A., 2014. Brain activity in response to visual symmetry. Symmetry 6 (4), 975–996. http://doi.org/10.3390/sym6040975.

Bertamini, M., Silvanto, J., Norcia, A.M., Makin, A.D.J., Wagemans, J., 2018. The neural basis of visual symmetry and its role in mid-level and high-level visual processing. Ann. N. Y. Acad. Sci. 1426, 111–126. http://doi.org/10.1111/nyas.13667.

Brainard, D.H., 1997. The psychophysics toolbox. Spatial Vis. 10, 433–436. https://doi.org/10.1163/156856897X00357.

Bulthé, J., Prinsen, J., Vanderauwera, J., Duyck, S., Daniels, N., Gillebert, C.R., Mantini, D., Op de Beeck, H.P., De Smedt, B., 2018. Multi-method brain imaging reveals impaired representations of number as well as altered connectivity in adults with dyscalculia. Neuroimage (in press). https://doi.org/10.1016/j.neuroimage.2018.06.012.

Chen, C.-C., Kao, K.-L.C., Tyler, C.W., 2007. Face configuration processing in the human brain: The role of symmetry. Cerebr. Cortex 17 (6), 1423–1432. http://doi.org/10.1093/cercor/bhl054.

Dale, A.M., 1999. Optimal experimental design for event-related fMRI. Hum. Brain Mapp. 8, 109–114.

Dale, A.M., Fischl, B., Sereno, M.I., 1999. Cortical surface-based analysis. Neuroimage 9 (2), 179–194. http://doi.org/10.1006/nimg.1998.0395.

Fischl, B., Dale, A.M., 2000. Measuring the thickness of the human cerebral cortex from magnetic resonance images. Proc. Natl. Acad. Sci. Unit. States Am. 97 (20), 11050–11055. http://doi.org/10.1073/pnas.200033797.

Fischl, B., Sereno, M.I., Dale, A.M., 1999. Cortical surface-based analysis. Neuroimage 9 (2), 195–207. http://doi.org/10.1006/nimg.1998.0396.

Friston, K.J., Zarahn, E., Josephs, O., Henson, R.N.A., Dale, A.M., 1999. Stochastic designs in event-related fMRI. Neuroimage 10 (5), 607–619. http://doi.org/10.1006/nimg.1999.0498.

Giannouli, V., 2013. Visual symmetry perception. Encephalos 50, 31–42.

Greve, D.N., Van der Haegen, L., Cai, Q., Stufflebeam, S., Sabuncu, M.R., Fischl, B., Brysbaert, M., 2013. A surface-based analysis of language lateralization and cortical asymmetry. J. Cognit. Neurosci. 25 (9), 1477–1492. http://doi.org/10.1162/jocn_a_00405.

Julesz, B., 1971. Foundations of Cyclopean Perception. The University of Chicago Press, Chicago, ISBN 0-226-41527-9.

Keefe, B.D., Gouws, A.D., Sheldon, A.A., Vernon, R.J.W., Lawrence, S.J.D., McKeefry, D.J., Wade, A.R., Morland, A.B., 2018. Emergence of symmetry selectivity in the visual areas of the human brain: fMRI responses to symmetry presented in both frontoparallel and slanted planes. Hum. Brain Mapp. http://doi.org/10.1002/hbm.24211.

Kohler, P.J., Clarke, A., Yakovleva, A., Liu, Y., Norcia, A.M., 2016. Representation of maximally regular textures in human visual cortex. J. Neurosci. 36 (3), 714–729. http://doi.org/10.1523/JNEUROSCI.2962-15.2016.

Kubilius, J., Baeck, A., Wagemans, J., Op de Beeck, H.P., 2015. Brain-decoding fMRI reveals how wholes relate to the sum of parts. Cortex 72, 5–14. http://doi.org/10.1016/j.cortex.2015.01.020.

Kubilius, J., Wagemans, J., Op de Beeck, H.P., 2011. Emergence of perceptual Gestalts in the human visual cortex: The case of the configural-superiority effect. Psychol. Sci. 22 (10), 1296–1303. https://doi.org/10.1177/0956797611417000.

Makin, A.D.J., Rampone, G., Pecchinenda, A., Bertamini, M., 2013. Electrophysiological responses to visuospatial regularity. Psychophysiology 50, 1045–1055. http://doi.org/10.1111/psyp.12082.

Makin, A.D.J., Rampone, G., Wright, A., Martinovic, J., Bertamini, M., 2014. Visual symmetry in objects and gaps. J. Vis. 14 (3), 1–12. http://doi.org/10.1167/14.3.12.

Makin, A.D.J., Wright, D., Rampone, G., Palumbo, L., Guest, M., Sheehan, R., Cleaver, H., Bertamini, M., 2016. An electrophysiological index of perceptual goodness. Cerebr. Cortex 26 (12), 4416–4434. http://doi.org/10.1093/cercor/bhw255.

Marr, D., 1982. Vision: A computational investigation into the human representation and processing of visual information. W.H. Freeman, San Francisco.

Misaki, M., Kim, Y., Bandettini, P.A., Kriegeskorte, N., 2010. Comparison of multivariate classifiers and response normalizations for pattern-information fMRI. Neuroimage 53 (1), 103–118. http://doi.org/10.1016/J.NEUROIMAGE.2010.05.051.

Osorio, D., 1996. Symmetry detection by categorization of spatial phase, a model. Proc. Biol. Sci. 263 (1366), 105–110. http://doi.org/10.1098/rspb.1996.0017.

Osorio, D., Cuthill, I., 2015. Camouflage and perceptual organization in the animal kingdom. In: Wagemans, J. (Ed.), The Oxford Handbook of Perceptual Organization. Oxford University Press, Oxford, pp. 843–862 (Oxford Library of Psychology). http://doi.org/10.1093/oxfordhb/9780199686858.013.044.

Poirier, F.J.A.M., Wilson, H.R., 2010. A biologically plausible model of human shape symmetry perception. J. Vis. 10, 9. http://doi.org/10.1167/10.1.9.

Pramod, R.T., Arun, S.P., 2018. Symmetric objects become special in perception because of generic computations in neurons. Psychol. Sci. 29, 95–109. http://doi.org/10.1177/0956797617729808.

Rhodes, G., Peters, M., Lee, K., Morrone, M.C., Burr, D., 2005. Higher-level mechanisms detect facial symmetry. Proc. Biol. Sci. 272 (1570), 1379–1384. http://doi.org/10.1098/rspb.2005.3093.

Royer, F.L., 1981. Detection of symmetry. J. Exp. Psychol. Hum. Percept. Perform. 7 (6), 1186–1210. http://doi.org/10.1037/0096-1523.7.6.1186.

Sasaki, Y., Vanduffel, W., Knutsen, T., Tyler, C., Tootell, R., 2005. Symmetry activates extrastriate visual cortex in human and nonhuman primates. Proc. Natl. Acad. Sci. Unit. States Am. 102 (8), 3159–3163. http://doi.org/10.1073/pnas.0500319102.

Tootell, R.B., Reppas, J.B., Kwong, K.K., Malach, R., Born, R.T., Brady, T.J., Rosen, B.R., Belliveau, J.W., 1995. Functional analysis of human MT and related visual cortical areas using magnetic resonance imaging. J. Neurosci.: Offic. J. Soc. Neurosci 15 (4), 3215–3230.

Treder, M.S., 2010. Behind the looking-glass: A review on human symmetry perception. Symmetry 2 (3), 1510–1543. http://doi.org/10.3390/sym2031510.

Tyler, C.W., Baseler, H.A., Kontsevich, L.L., Likova, L.T., Wade, A.R., Wandell, B.A., 2005. Predominantly extra-retinotopic cortical response to pattern symmetry. Neuroimage 24 (2), 306–314. http://doi.org/10.1016/j.neuroimage.2004.09.018.

Wagemans, J., Van Gool, L., Swinnen, V., Van Horebeek, J., 1993. Higher-order structure in regularity detection. Vis. Res. 33 (8), 1067–1088. http://doi.org/10.1016/0042-6989(93)90241-N.

Wagemans, J., 1997. Characteristics and models of human symmetry detection. Trends Cognit. Sci. 1 (9), 346–352. http://doi.org/10.1016/S1364-6613(97)01105-4.

Winawer, J., Horiguchi, H., Sayres, R.A., Amano, K., Wandell, B.A., 2010. Mapping hV4 and ventral occipital cortex: The venous eclipse. J. Vis. 10 (5), 1. http://doi.org/10.1167/10.5.1.

Witthoft, N., Nguyen, M.L., Golarai, G., LaRocque, K.F., Liberman, A., Smith, M.E., Grill-Spector, K., 2014. Where is human V4? Predicting the location of hV4 and VO1 from cortical folding. Cerebr. Cortex 24 (9), 2401–2408. http://doi.org/10.1093/cercor/bht092.

Wright, D., Makin, A.D.J., Bertamini, M., 2015. Right-lateralized alpha desynchronization during regularity discrimination: Hemispheric specialization or directed spatial attention? Psychophysiology 52 (5), 638–647. http://doi.org/10.1111/psyp.12399.

Wright, D., Makin, A.D.J., Bertamini, M., 2017. Electrophysiological responses to symmetry presented in the left or in the right visual hemifield. Cortex 86, 93–108. http://doi.org/10.1016/J.CORTEX.2016.11.001.

Zhu, T., 2014. Neural processes in symmetry perception: a parallel spatio-temporal model. Biol. Cybern. 108 (2), 121–131. http://doi.org/10.1007/s00422-013-0578-y.